Neuron, Vol. 32, 565–577, November 20, 2001, Copyright ©2001 by Cell Press

Visual Motion Processing Investigated Using Contrast Agent-Enhanced fMRI in Awake Behaving Monkeys

Neurotechnique

Wim Vanduffel,[1,4] Denis Fize,[1]
Joseph B. Mandeville,[3] Koen Nelissen,[1]
Paul Van Hecke,[2] Bruce R. Rosen,[3]
Roger B.H. Tootell,[3] and Guy A. Orban[1]
[1] Laboratorium voor Neuro- en Psychofysiologie
Katholieke Universiteit Leuven
Campus Gasthuisberg
Herestraat 49
[2] Afdeling Radiologie
UZ Gasthuisberg
B-3000 Leuven
Belgium
[3] NMR Center
Massachusetts General Hospital
Charlestown, Massachusetts 02129

Summary

To reduce the information gap between human neuroimaging and macaque physiology and anatomy, we mapped fMRI signals produced by moving and stationary stimuli (random dots or lines) in fixating monkeys. Functional sensitivity was increased by a factor of ~5 relative to the BOLD technique by injecting a contrast agent (monocrystalline iron oxide nanoparticle [MION]). Areas identified as motion sensitive included V2, V3, MT/V5, vMST, FST, VIP, and FEF (with moving dots), as well as V4, TE, LIP, and PIP (with random lines). These regions sensitive for moving dots are largely in agreement with monkey single unit data and (except for V3A) with human fMRI results. Moving lines activate some regions that have not been previously implicated in motion processing. Overall, the results clarify the relationship between the motion pathway and the dorsal stream in primates.

Introduction

For decades, the macaque monkey has been an important model for understanding information processing in the human visual system. Indeed, most of our current knowledge about the functional organization of the primate brain has been derived from invasive methods in macaques, which cannot be directly applied to humans. Recently, noninvasive imaging tools (e.g., positron emission tomography [PET], functional magnetic resonance imaging [fMRI], and magneto-encephalography [MEG]) have furnished additional physiological information from the human visual system, be it at coarse temporal and/or spatial resolution relative to invasive methods in macaques. In order to bridge the gap between these different experimental approaches to study primate visual cortex (e.g., macaque single units, human fMRI, human psychophysics, monkey connectional data, etc.), we developed fMRI methods to map activity in the visual cortex of the awake macaque.

[4] Correspondence: wim.vanduffel@med.kuleuven.ac.be

Until now, several reports have demonstrated that fMRI is feasible in monkeys (Logothetis et al., 1999, 2001; Dubowitz et al., 1998; Stefanacci et al., 1998; Vanduffel et al., 1998; Disbrow et al., 2000; Hayashi et al., 1999); here, we proceeded to develop and improve *awake* monkey fMRI techniques. The best detection sensitivity to date was undoubtedly obtained by Logothetis and colleagues (1999, 2001) in anesthetized animals, using a specially designed vertical bore 4.7 Tesla magnet. However, since 1.5T scanners are more commonly available, we proceeded to develop and improve awake monkey fMRI techniques using a low-field scanner.

In order to achieve this goal, we had to combat the small amplitude of blood oxygen level-dependent (BOLD) signal changes at 1.5 Tesla (see below). Therefore, we turned to MRI contrast agents (dextran-coated iron oxide agents; MION) with long blood half-lifes (Weissleder et al., 1990; Josephson et al., 1990). In anesthetized rodents, such agents have been shown to increase the sensitivity for detecting brain activation relative to conventional BOLD signals (Mandeville et al., 1998; Van Bruggen et al., 1998). Moreover, functional MION signal changes are larger in brain parenchyma than in large vessels (Mandeville and Marota, 1999), whereas the opposite holds for BOLD signals (at 1.5T). Thus, in principle, contrast agents should produce better localized maps relative to "low-field" BOLD imaging (i.e., the large blood vessel artifacts are largely reduced in contrast agent imaging).

We chose to apply this imaging strategy to a simple visual motion paradigm, used extensively in human functional imaging (Zeki et al., 1991; Tootell et al., 1995; Sunaert et al., 1999; Goebel et al., 1998). In fixating monkeys, we presented random dot and random line stimuli that were either coherently moving or static. Applying identical stimuli to monkeys allows us to compare fMRI motion sensitivity to the incidence of direction-selective neurons in these regions (e.g., Andersen, 1997; Orban, 1996). This selectivity is the hallmark of motion processing regions and has been assessed extensively in single-cell recordings (which usually explore only a single cortical region). In contrast, fMRI enabled us to explore the complete motion pathway in single awake animals, to assess the degree to which this pathway conforms to the widely accepted concept of a "dorsal stream" (Ungerleider and Mishkin, 1982) and to compare motion sensitivity for different types of stimuli.

Furthermore, fMRI measures of motion sensitivity should clarify the functional homology between cortical visual areas in macaques and humans. For instance, area MT/V5+ in human cortex has been assumed homologous to area MT/V5 (Tootell et al., 1995; Zeki et al., 1991) and satellite areas (e.g., MST) in macaques. However, it has never been tested using the same technique and experimental paradigm whether MT/V5+ shows the expected degree of motion sensitivity in both species. A related question is whether the additional motion-sensitive areas described in humans (e.g., Dupont et al., 1994; Goebel et al., 1998) can be functionally isolated in macaque cortex. Finally, motion sensitivity

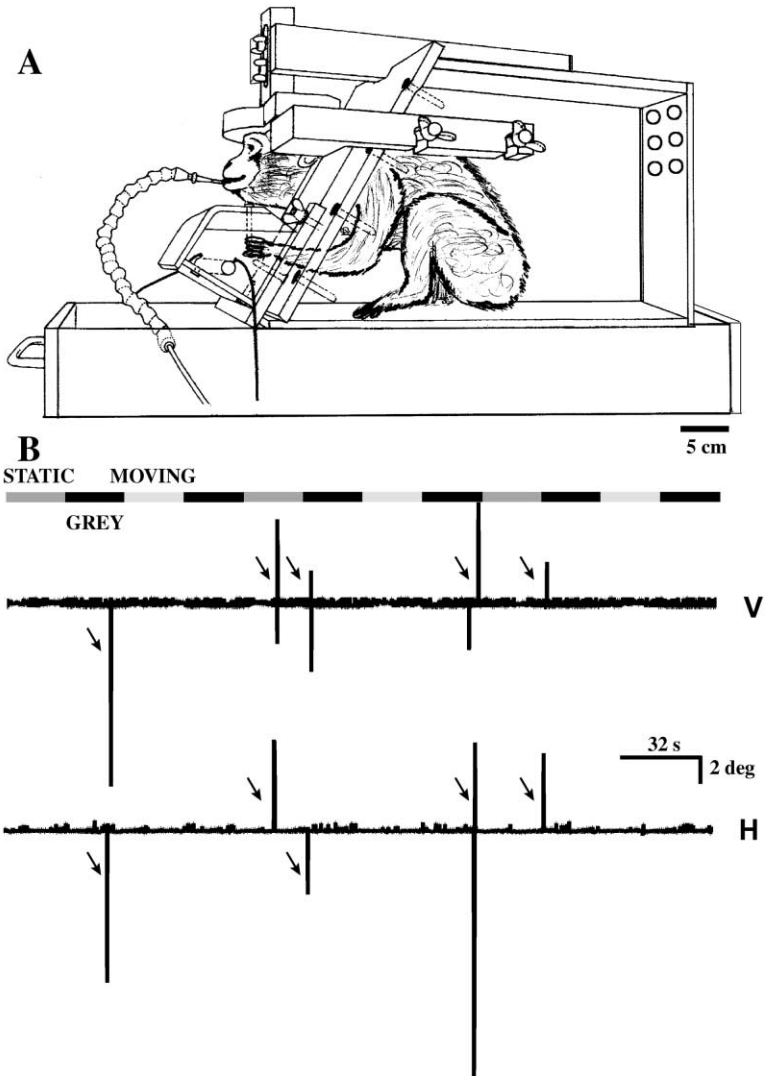

Figure 1. MR Compatible Monkey Chair and Eye Position Recordings

(A) Diagram of the monkey in the MR scanner. The monkey sat on its haunches in a plastic restraint box with its head immobilized comfortably but securely, directly beneath a radial surface coil.

(B) 276 s long horizontal and vertical eye position recordings (M3) obtained with an infrared corneal reflection system (Iscan) during fMRI scanning. Illustrated recordings were representative. Arrows indicate saccades.

has been observed repeatedly in fMRI studies of human V3A (Tootell et al., 1997; Sunaert et al., 1999), but this motion sensitivity is inconsistent with single unit studies that reported little motion selectivity in macaque V3A (Gaska et al., 1988; Joris et al., 1997). This inconsistency can be resolved using fMRI in macaques.

Results

Three macaque monkeys (M1-3), each implanted with MR-compatible headsets, were adapted to restraint in a natural "sphinx" position, facing parallel with the horizontal bore of a conventional MR scanner (Figure 1A). Fixation was controlled in M1 and M2 using a high acuity fixation task and in M3 by recording eye positions. In monkeys M1 and M3, we injected MION intravenously before scanning. Moving or stationary stimuli were presented on a transparent screen positioned in the bore of the magnet. Moving/stationary conditions were presented in blocks, typically in alternation with a uniform gray screen. In total, 37,200 functional brain volumes in M1 (acquired during three MION and five BOLD sessions) and 26,800 in M3 (eight MION sessions) were analyzed using SPM99 and FreeSurfer. Many more functional volumes ($\sim$160,000) were acquired during 49 BOLD-sessions in M1 and 13 BOLD sessions in M3, which yielded functional MRI data unrelated to those of the present study.

Behavioral Performance Levels

We assessed fixation accuracy in M3 by directly measuring the horizontal and vertical eye position during each scan session. Representative horizontal and vertical eye traces are shown in Figure 1B. In these examples, the monkey interrupted fixation only $\sim$5 times (indicated by the arrows) during these 276 s long scans. In the experiments analyzed for the present study, monkey M3 fixated for 85%–92% of the total experimental duration within a fixation window of $2^\circ \times 2^\circ$. Percent fixation did not differ between the moving and stationary conditions ($p = 0.099$, two-tailed t test).

M1 (and M2) typically achieved 98%–100% correct in the high acuity fixation task throughout each scan. M1's performance levels were very similar in the MION experi-

ments (98.5% ± 2.9% correct) and in comparable BOLD experiments (99.4% ± 1.8%). Fixation task performance exceeded that of three motivated human subjects who performed an identical fixation task (95.5% ± 2.5%). When the same human subjects were instructed to maintain fixation on points peripheral to the orientation target, performance accuracy decreased significantly to 82.8% ± 6.5% and 65.7% ± 9.5% for 1.3° and 2.5° eccentricity, respectively. Thus, subjects had to carefully maintain fixation on the central target in order to achieve maximum performance accuracy.

Direct offline eye position measurements in the mock scanner showed that M1 fixated within a window of 2° × 2° during 75% of the total experimental duration. There were no significant differences in percent fixation between the different conditions (75.3% ± 2.7%, 78.7% ± 2.4% for the stationary and moving stimulus condition, respectively; $p = 0.062$, t test).

Side Effects of MION

No statistically significant difference was observed between performance levels of monkey M1 in the high acuity fixation task during the last BOLD session (98.3% ± 5.4%) preceding the MION injection and the first MION session (99.5% ± 2.8%) ($p > 0.22$, two-tailed t test). Monkey M3 also performed equally well, before (89% fixation) and after the first MION injection (85% fixation). These high performance levels suggest that an effective dose of intravenously administered MION does not result in obvious short-term behavioral and/or cognitive effects.

Moreover, we observed no obvious negative health effects in two monkeys in which we injected MION, up to 10 months after the first injection. In total, M1 and M3 received 60 and 128 mg/kg MION, respectively. After repeated MION injections, we did observe a marked increase in the saturation levels of the protein transferrin (which is linked to the iron metabolism), as well as in iron plasma levels. Those values were ~10 times higher than normal after a series of three to seven daily MION sessions. However, treatment with an iron chelator (2× 0.5 mg/day, i.m., deferoxaminum, Desferal®, Novartis, Brussels) for 4–6 days restored normal plasma iron and transferrin saturation levels.

Functional Sensitivity of MION

To measure the gain in sensitivity obtained with the contrast agent, we compared MION and BOLD signal changes when monkeys fixated either moving or stationary patterns composed of either random dots or lines. Results from both macaque single unit recordings and human functional imaging predicted that area MT/V5+ (MT/V5 and its satellites MST and FST [Desimone and Ungerleider, 1986]) should be activated most profoundly by moving compared to stationary stimuli; thus, we concentrated on these regions in the comparison between BOLD and MION.

Signal Amplitude

The average BOLD and MION signal changes for area MT/V5 of M1 are plotted in Figure 2A. Note that MION-weighted T_2^* signal changes were opposite in sign to BOLD signals (see Experimental Procedures). The MR signal change between the moving and the stationary

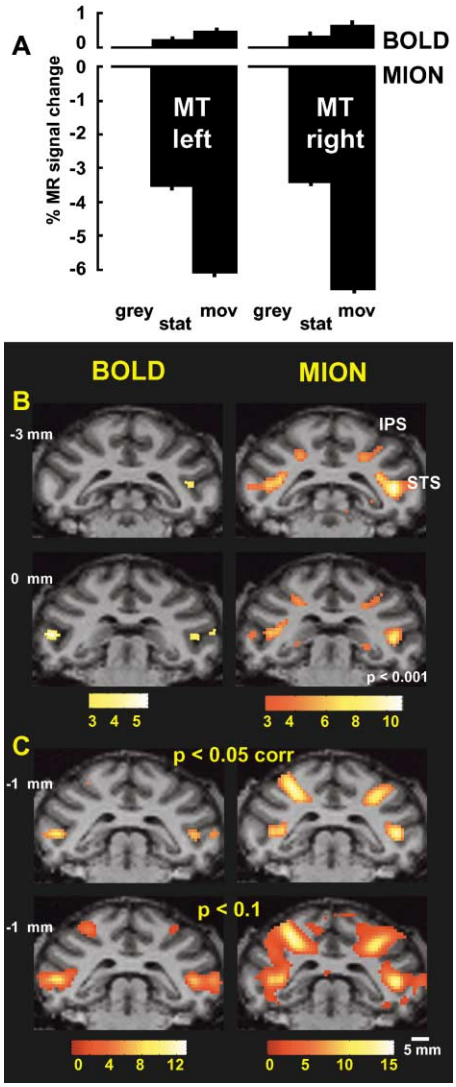

Figure 2. Comparison of MION with BOLD MR Signals (M1)

(A) The average percent MR signal change in left and right area MT/V5 (seven voxels surrounding the local maxima) with respect to the no stimulus condition (gray) for the three stimulus conditions (moving [mov] and stationary [stat] dots, no stimulus). The same number of functional volumes (120) were acquired in the MION and BOLD experiments. Lines indicate standard errors of the mean.

(B and C) Statistical parametric maps comparing moving versus stationary random dots (B) and random lines (C) for BOLD (left-hand side) and MION (right-hand side) fMRI signals in coronal sections taken slightly anterior to area MT/V5. The exact level is indicated in millimeters with respect to the interaural plane (negative values are posterior). The color scales indicate the t scores. Thresholds were $p < 0.001$ uncorrected for multiple comparisons (B) and $p < 0.05$ corrected and $p < 0.1$ uncorrected (C). IPS, intraparietal sulcus; STS, superior temporal sulcus.

condition was 0.29% ± 0.03% (mean ± SEM) in this BOLD experiment and 3.00% ± 0.09% in the corresponding MION experiment. Thus, the use of an iron oxide contrast agent increased percent MR signal changes by a factor of ten in area MT/V5, at least under our experimental conditions. These observations for area MT/V5 also generalized throughout visual cortex of monkey M1. Averaging over five motion-sensitive re-

gions including area MT/V5 MR signal changes increased by a median factor of eight (interquartile range of 3.9) for the moving to stationary comparison, and a median factor of ten (interquartile range of 4.2) for the moving to no stimulus comparison.

Although we obtained similar BOLD signals (0.67% ± 17%) for the comparison of moving versus stationary dots in MT/V5 of a second monkey (M2), no reliable signals could be measured in any of the ten BOLD scanning sessions of monkey M3 in which we acquired functional volumes at a resolution of 3 × 3 × 3 mm (reflecting inadequate performance or idiosyncratic differences between subjects). In contrast to the large differences in BOLD signals between M1 and M3, MION signals were at least as large in M3 compared to M1 (see below for quantitative data).

Statistical Power

The gain in signal change was accompanied by an increase in statistical power: the t scores of the activity maps reached much higher values for MION than for BOLD (Figures 2B and 2C). The BOLD and the MION experiments were equated as much as possible. The same moving-stationary stimuli were used, the same total number of functional brain volumes were acquired (120 and 480 per condition for Figures 2B and 2C, respectively), and the activity maps were thresholded at the same level of $p < 0.001$, uncorrected. We observed bilateral motion-selective MION activation in the superior temporal sulcus (STS) and the fundus of the intraparietal sulcus (IPS). At this low statistical threshold, we even observed bilateral motion sensitivity in the pulvinar (section at 0 mm). These bilateral MION activations were much more significant (notice difference in color scales) than the corresponding BOLD activation patterns, which could even appear unilateral (e.g., STS at −3 mm) or nonsignificant (e.g., IPS and the pulvinar).

Figure 2C extends these observations to random lines and to the acquisition of a larger number of functional volumes. The MION and BOLD activity maps are sharply defined: t values decrease steadily from local maxima, indicating that MION and BOLD activation sites are well defined. However, as the figure demonstrates, the activation pattern obtained by lowering the threshold ($p < 0.1$) in the BOLD activity map is still reduced (see IPS) compared to those obtained with MION at a threshold corrected for multiple comparisons. Although t scores of the local maxima obtained in this MION experiment were 10.88 (MT/V5) and 6.77 (VIP), this single section (selected for the IPS activation) might give the erroneous impression that the IPS activation by lines is stronger than the STS activation.

Anatomical Localization

In addition to increasing statistical power and signal changes, MION appeared to improve the anatomical accuracy of the activation patterns. Figure 3A shows a sagittal slice through the STS, revealing two nearly distinct motion-sensitive foci. The BOLD experiment revealed that the posterior activation site ($p < 0.05$ corrected) was completely centered over the posterior bank of the STS (green arrows in Figures 3Ba and 3Bb). The corresponding MION maps showed an activation pattern that nicely fitted the curvature of gray matter in the posterior bank (green arrow) and the floor of the STS (pink arrows in Figures 3Ca and 3Cb). At the most posterior level (Figure 3Ca), the activation of the posterior bank was even segregated from that in the floor of the STS, suggesting that two different areas were engaged by the moving dots (see below for their identification). It appears as if the activation site of the BOLD map was centered over the center of mass of the corresponding MION sites. Moreover, at more anterior levels, the focus in the BOLD maps expanded toward the lip of the sulcus (compare Figures 3Bc and 3Bd with Figures 3Cc and 3Cd), possibly evoked by BOLD signals originating from the large draining vessels overlaying the STS. Thus, although exactly the same imaging parameters were applied in the BOLD and the MION experiments, the use of MION appears to improve the spatial specificity of the activation maps.

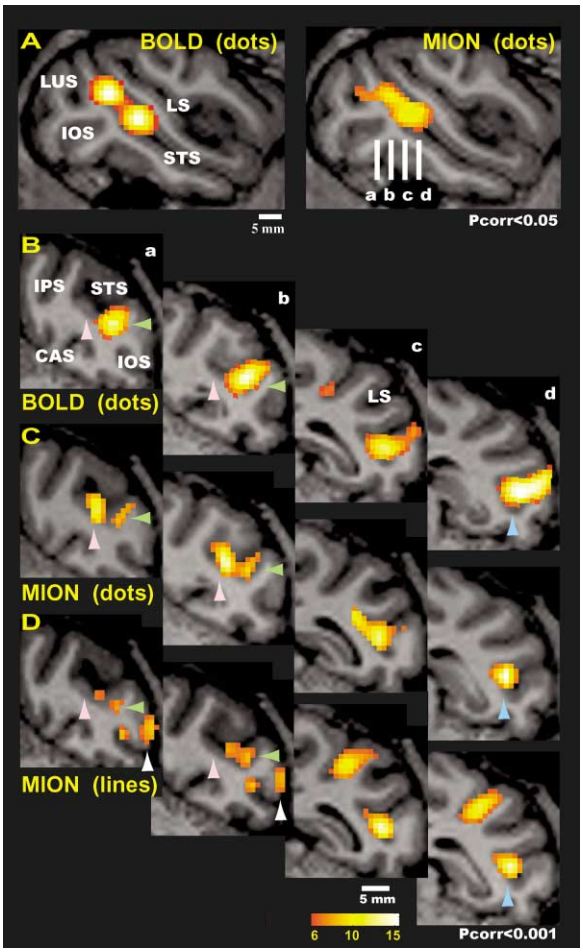

Figure 3. Improved Anatomical Localization of MION Relative to BOLD MR Responses (M1)

BOLD and MION statistical maps for the comparison between moving and stationary random dots (A–C) and lines (D) in a sagittal section ([A], threshold $p < 0.05$ corrected) and four coronal sections ([B]–[D], threshold $p < 0.001$ corrected), as indicated by the labels (a)–(d) on the right-hand side of panel (A). Color scales indicate t scores. The number of analyzed functional volumes was much larger for the BOLD (1280) than for the MION (300) experiment. However, similar results were obtained with an equal number of volumes (300) acquired during the BOLD experiments but applying a lower statistical threshold. Pink arrows point to the floor of the STS (vMST), green to MT/V5, blue to FST (at level d), and white to V4. CAS, calcarine sulcus; LUS, lunate sulcus; IOS, inferior occipital sulcus; LS, lateral sulcus.

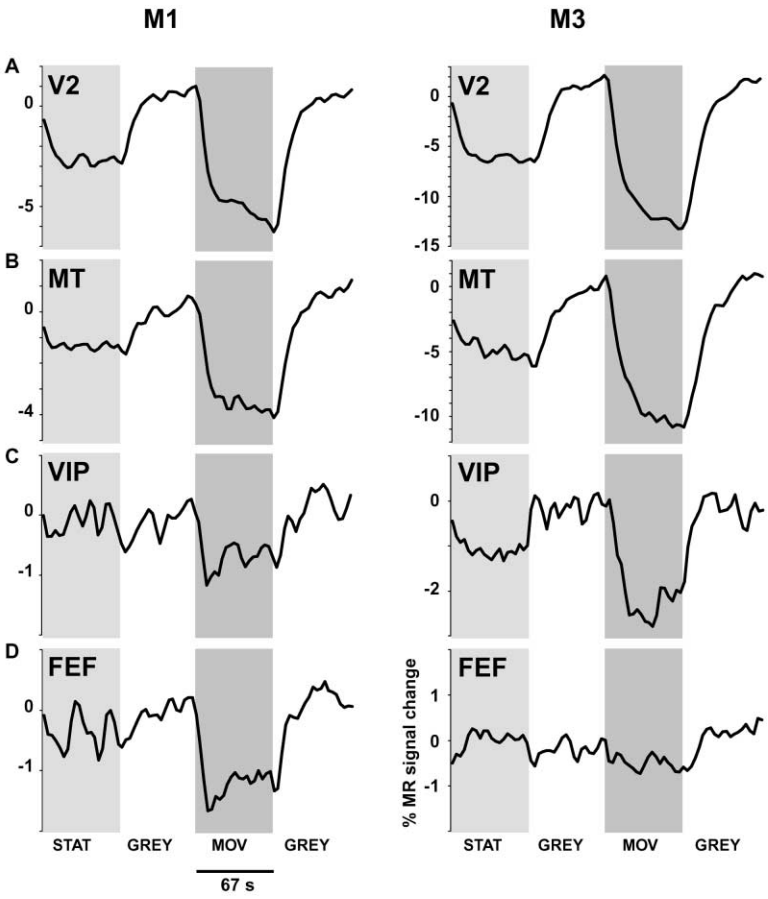

Figure 4. Time Courses in Areas V2, MT/V5, VIP, and FEF

MION time courses for areas V2 (A), MT/V5 (B), VIP (C), and FEF (D) of monkeys M1 (left) and M3 (right) for two stimulus conditions (stationary dots, STAT; moving dots, MOV) and a no stimulus condition (GRAY). Data are averages from the two hemispheres, including seven voxels surrounding the local maximum per hemisphere, derived from 300 functional volumes. In all areas and hemispheres, the moving-stationary difference reached significance ($p < 0.05$ corrected).

Identification of Motion-Sensitive Regions

Using the MION method, we could reliably identify several motion-sensitive regions in the macaque brain, including posterior occipital areas, such as V2 (Figure 4A); regions in the STS, such as MT/V5 (Figure 4B); regions in the IPS, such as VIP (Figure 4C); and regions outside the classical visual cortex, such as FEF (Figure 4D). In agreement with their position in the cortical hierarchy (Felleman and Van Essen, 1991, for discussion, see below), we observed smaller MR signal changes in VIP (0.6% using dots and 1.0% using lines, averaged over the two monkeys) and in FEF (0.7% using dots and 1.0% using lines) relative to MT/V5 (3.4% using dots and 2.2% using lines) and V2 (4.5% using dots and 0.8% using lines). Despite these differences in MR signal changes, all cortical regions motion sensitive for moving dots were also motion sensitive for moving lines. Thus, motion sensitivity for random lines will be described below only for those areas in which moving dots were ineffective.

Posterior Occipital Areas: V2 and V3

In area V2 (especially the dorsal subdivision on the posterior bank of the lunate sulcus), we observed profound motion sensitivity (blue line in Figure 5, see also Figure 6). Differential MR signals between the moving and stationary condition reached 5% and reached 14% between the no stimulus and the moving stimulus condition. Deeper in the lunate sulcus, we observed weaker motion sensitivity (red line in Figure 5), which we attribute to area V3. Close to the fundus of the inferior occipital sulcus we also observed motion sensitivity (green line in Figure 5) which probably reflects V2 ventral but might include VP.

Superior Temporal Areas

Taking advantage of the increased spatial specificity obtained with MION (see Figure 3) and guided by the known anatomical location of the subcompartments of monkey-MT/V5+, we tried to distinguish between the different areas *within* the monkey-MT/V5+ complex. As shown in Figure 3Ca, the MION maps of the right hemisphere of monkey M1 yielded an activation in the posterior bank of the STS (green arrow), separated from activation in the floor of the STS (pink arrow). Anatomically, the former focus corresponds to area MT/V5, while the focus in the floor of the STS appears to correspond to area vMST, as described by Tanaka et al. (1993). At progressively more anterior levels in the STS, this separation remains visible as two local maxima in the statistical maps. As expected by the extent of the stimulated portion of area MT/V5, the posterior bank activation disappears between levels b and c. The activation patterns obtained using the moving line stimuli (see Figure 3D) supported this distinction between vMST and MT/V5. Unlike the moving dots, line stimuli activated the posterior bank (MT/V5, green arrow) but not the floor of the STS (vMST, red arrow) at levels a and b. The separation between MT/V5 and vMST using moving dots is further documented in Figure 7 for the left hemisphere of M1 and the right hemisphere of M3 (in standard exper-

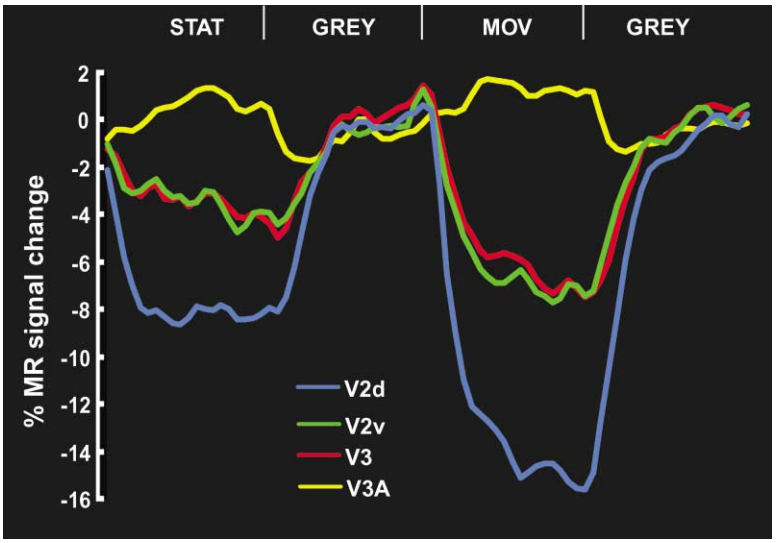

Figure 5. Motion Sensitivity in Prestriate Areas (M3)

MION time courses for areas V2d (blue line), V3 (red line), V2v (green line), and V3A (yellow line) of monkey M3 (right hemisphere) for two stimulus conditions (stationary dots, STAT; moving dots, MOV) and a no stimulus condition (GRAY). The data are derived from 380 functional volumes.

iments with voxel size of 27 mm^3, Figures 7A and 7B) and for left and right hemisphere of M3 (in additional experiments with 8 mm^3 voxels, Figures 7C and 7D). Thus, the MION maps suggest not only an *anatomical* but also a *functional* separation between MT/V5 and vMST, within the monkey-MT/V5+complex.

The moving dot and line stimuli also activated another region within the STS, which was located just anteroventral to area MT/V5. This ventral satellite can be observed in a sagittal view of the STS, together with the MT/V5 site (Figure 3A), as well as in the coronal sections at levels c and d (blue arrows in Figures 3C and 3D). This ventral activation was centered on the dorsal-most portion of the floor of the STS. Based on its anatomical localization, this latter region might correspond to area FST.

With moving random lines, the motion-sensitive activation extended beyond the STS in the prelunate gyrus corresponding to V4d (Figures 3D, white arrow, and 6C). In addition, a small but consistent activation was observed further ventrally on the lateral convexity of inferotemporal cortex, near the posterior middle temporal sulcus (Figure 6C).

Intraparietal Areas

Macaque VIP contains a high percentage of direction-selective cells and receives direct input from area MT/V5 (Maunsell and Van Essen, 1983; Colby et al., 1993). It has been localized deep within the intraparietal sulcus, approximately midway along its length. Based on its location and its functional properties, the motion-sensitive region in the IPS observed with dots (Figure 2B) may be equivalent to area VIP.

We consistently observed more widespread activation (in terms of spatial extent, response amplitude, and statistical significance) within the IPS when using moving lines compared to moving dots (e.g., compare Figures 2B and 2C, and Figures 6B and 6C). Moving random lines not only activated area VIP, but also the lateral bank of the IPS at more caudal locations. Based upon their locations, these regions most likely correspond to areas LIP and PIP.

Areas outside Classical Visual Cortex

We also observed motion-sensitive responses in several regions *outside* classical visual cortex. One region (FEF) was located in the anterior bank of the arcuate sulcus (Figure 6). Consistent with the high motion sensitivity in the IPS for line stimuli and with the profound input from intraparietal regions to the FEF (Schall et al., 1995), we also observed higher motion sensitivity for lines than for dots in the latter area (see Figure 6C). The difference in amplitude of the signal change in FEF between the two monkeys might be attributed to the difference in the fixation paradigm in M1 and M3.

In two additional areas, we observed significant bilateral motion sensitivity ($p < 0.05$ corrected) in only one of the monkeys. In monkey M3, the dorsal portion of the posterior bank of the lateral sulcus was motion sensitive for both dots and lines (see Figures 6B and 6C). A similar activation has been observed in the human lateral sulcus (Sunaert et al., 1999). In monkey M1, the pulvinar complex was also motion sensitive (Figure 2B).

Area V3A

We did not observe significant motion-sensitive voxels in area V3A, irrespective of whether motion sensitivity was tested with dots or lines. In addition, we sampled activity from macaque V3A, as defined by gyral/sulcal location rather than by functional tests. Since V3A is relatively wide ($\sim$9 mm width) and its gyral location is stable, the V3A region of interest was safely localized. In this region, the moving and stationary stimulus conditions produced essentially equal fMRI activation (yellow line in Figure 5). In fact, the MION signal in area V3A increased slightly during these two conditions, in comparison to the no stimulus control condition. Since statistical analysis with and without global scaling (see Experimental Procedures) yielded the same results, the increased MION signals during these stimulus conditions (which amount to a deactivation) cannot be attributed to global scaling.

Inter- and Intrasubject Reliability

As discussed above and summarized in Figure 6, both monkeys showed significant ($p < 0.05$ corrected) bilateral motion sensitivity for dot stimuli in the posterior bank and the fundus of the lunate sulcus (V2 and V3), the fundus of the inferior occipital sulcus, the posterior bank of the dorsal superior temporal sulcus (MT/V5, vMST, FST), the middle of the IPS, and the anterior bank

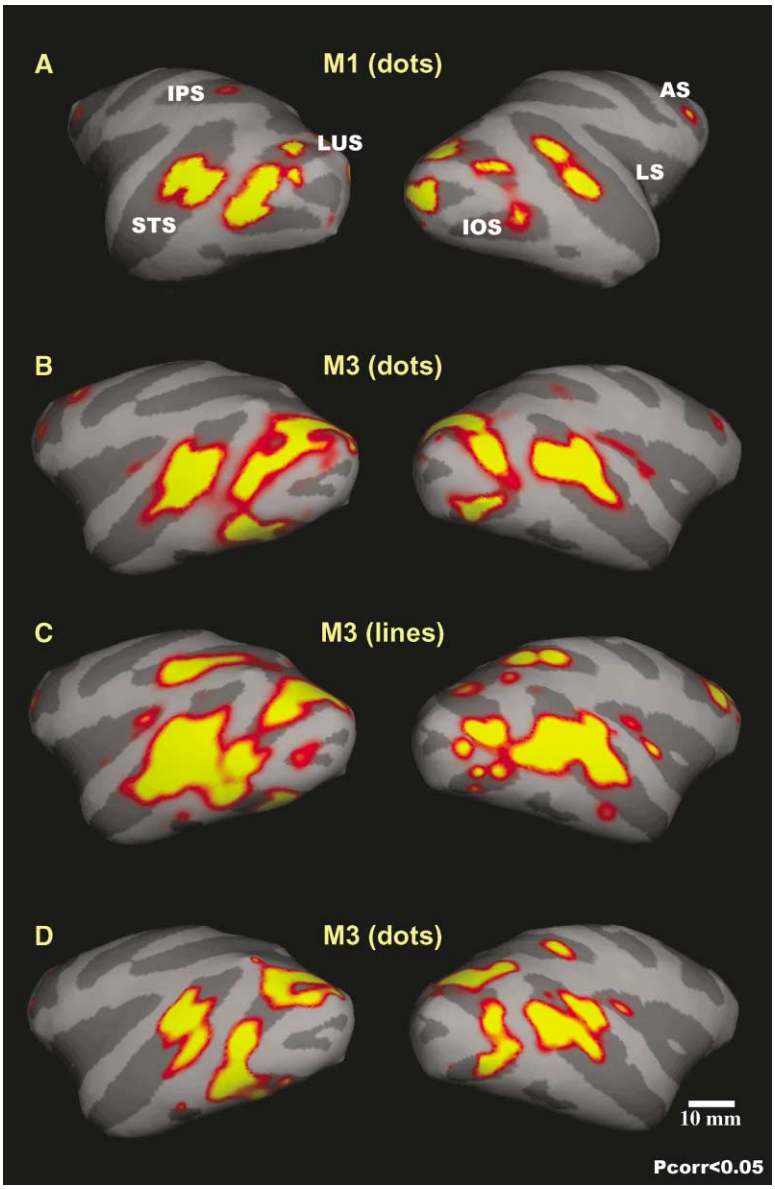

Figure 6. Topography of Motion Sensitivity on Inflated Hemispheres

Statistical maps for moving compared to stationary dots (A, B, and D) and lines (C) ($p < 0.05$ corrected) on a lateral view of the inflated left and right hemispheres of monkey M1 (A) and M3 (B–D). (D) Shows results from a similar experiment (3 weeks later) to that of (B). AS, arcuate sulcus; other abbreviations, see Figure 3. In right IPS of M1 and in left IPS of M3, the size of the activation was so small that it was not painted on the inflated hemispheres.

of the arcuate sulcus. The fact that bilateral activation foci were seen in the same cortical regions, in both monkeys (Figures 6A and 6B), suggests that our fMRI approach offers good intersubject reliability.

Figures 6B and 6D compares motion sensitivity in monkey M3 obtained in two different sessions, ~3 weeks apart. Although the number of functional volumes and the epoch duration differed between the two experiments, the activated voxels ($p < 0.05$, corrected for multiple comparisons) overlapped by 84% in both hemispheres.

Moving Dots and Lines

Motion sensitivity assessed with moving random dots decreased as a function of hierarchical level, especially beyond area MT/V5 (Figure 8). On the contrary, the regional distribution of motion sensitivity for random lines is much broader (see Figure 6C), with a maximum at intermediate hierarchical levels (see Figure 8). The relatively small standard errors of the mean (calculated across the four hemispheres) are a further indication of the inter- and intrasubject reliability.

Discussion

These fMRI studies on alert fixating monkeys proved surprisingly straightforward to accomplish. We used a conventional 1.5T scanner and near-standard behavioral and surgical procedures. We found that the use of an iron oxide contrast agent with a long blood half-life considerably enhanced functional brain imaging in awake, behaving primates.

Though our comparisons were understandably limited in this initial study, these procedures appeared to yield excellent reliability, both between and within subjects. Using MION, we were able to reveal a substantial portion of the motion pathway, which generally fits with the classical view of motion processing in dorsal stream areas. Specifically, areas V2, V3, MT/V5, vMST, FST, and VIP

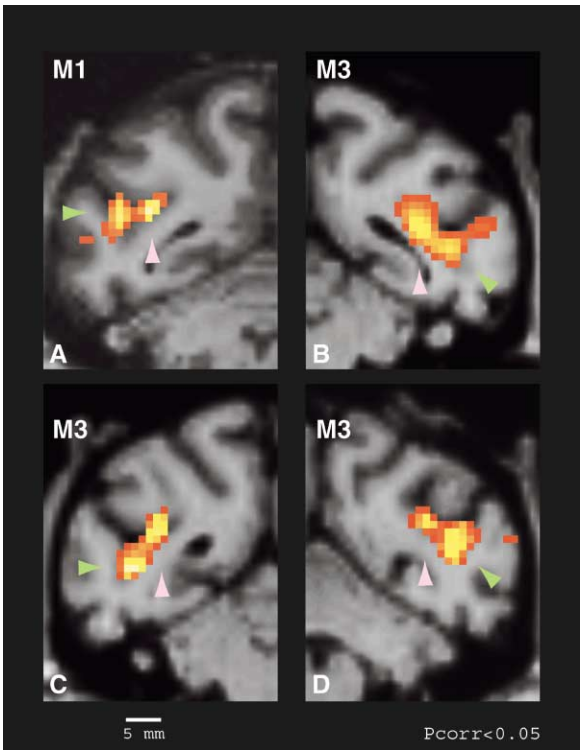

Figure 7. MT/V5—vMST Distinction Using MION

Statistical maps for moving compared to stationary dots in the left hemisphere of M1 (A) and right hemisphere of M3 (B). Data of panels (A) and (B) were acquired using a voxel size of $3 \times 3 \times 3$ mm. Panels (C) and (D) show the statistical maps of both hemispheres of M3 for the same stimulus comparison but from an experiment using 2 mm^3 isotropic voxels. Pink arrows point to the floor of the STS (vMST), and green arrows point to MT/V5.

proved to be motion sensitive. More unexpected motion-sensitive regions included areas PIP, LIP, FEF, V4, TE, portions of the lateral sulcus, and even the pulvinar. As predicted by the single-cell literature, macaque area V3A was *not* motion selective, unlike human area V3A.

MION as a Contrast Agent for Monkey fMRI

Both the BOLD and MION techniques are sensitive to the local concentration of contrast agent—deoxyhemoglobin in the former case and exogenous iron in the latter method. The local concentration of endogenous contrast agent (deoxyhemoglobin) decreases as venous blood becomes more oxygenated during activation, leading to an increase in BOLD signal. When enough iron oxide is used to overwhelm the BOLD effect, changes in oxygenation have a negligible effect on total blood magnetization. Thus, an increase in the local concentration of exogenous contrast agent (iron oxide) results from an increase in local cerebral blood volume, so activation-induced MION-based changes are negative rather than positive, as BOLD-based signal changes.

The contrast agent (MION) dose was selected in order to achieve the best trade-off between large percent signal changes (more agent) and a large signal-to-noise ratio (less agent); the optimal dose attenuates MR signals by about 50% at any echo time (Mandeville et al., 1998). The echo time used in this study was optimized for BOLD: the echo time was sufficiently large to produce good BOLD sensitivity, yet small enough to minimize susceptibility artifacts. We used the same echo time for the MION imaging, because it attenuated the signal by 50%. A small additional increase in sensitivity could have been obtained by using a smaller echo time with a larger dose of MION (Mandeville et al., 1998). To improve the statistical analysis of the MION experiments, we directly measured the MION impulse response function (see Figure 9 and Experimental Procedures).

The use of MION yielded approximately a 10-fold increase in the percent signal change relative to comparable BOLD measurements at 1.5T. Since the MR signal is attenuated by a factor of approximately two due to the MION, the improvement of the sensitivity (contrast-to-noise ratio) can be estimated as $0.5 \times 10 = 5$. This increase in sensitivity is in general agreement with an increased contrast-to-noise ratio of 5.7 in anesthetized rodents at 2T (Mandeville et al., 1998). Finally, the MION resulted in better statistical power and better spatial localization of the activated brain regions. The present data suggest that contrast agent-enhanced fMRI at low magnetic field strengths provides an excellent alternative to BOLD imaging at high magnetic fields.

The monkeys showed no obvious short-term adverse effects due to injection of the contrast agent. However, despite the encouraging clearance after the use of the iron chelator (deferoxamin), it remains an open question whether there are longer-term effects of chronic iron administration on the spleen, liver, and kidney, where MION accumulates (Schaffer et al., 1993).

Motion Sensitivity in the Macaque Visual System: Comparing fMRI and Single-Cell Studies

The cortical regions showing fMRI motion sensitivity correlate remarkably well with areas containing a high proportion of direction-selective neurons (for review, see Orban, 1996). Areas MT/V5, MST, VIP, and PO/V6 and layers 4B and 6 of area V1 contain more than 60% direction-selective neurons. Area V3 and the thick stripes of V2 have a proportion of direction-selective cells close to 40% (Felleman and Van Essen, 1987; Gegenfurtner et al., 1997; Levitt et al., 1994; Peterhans and Watson, 1993). In all these areas, we observed motion sensitivity, with the exception of PO/V6 and V1. We observed some activation of V1 (Figure 6), but this was not consistent across subjects/hemispheres. The weakness of these signals may reflect the narrow width of layers 4B and 6 or the nonoptimal speed of the stimuli used here (Orban et al., 1986; Mikami et al., 1986). The absence of a PO/V6 activation might be due to the restricted size of our stimuli compared to the requirements of the V6 neurons (Galletti et al., 1996). A similar explanation might apply to areas such as MSTd, 7a, and STP, which have previously been implicated in motion processing (Tanaka et al., 1986; Lagae et al., 1994; Siegel and Read, 1997; Oram and Perrett, 1994) and are preferentially activated by larger and more complex stimuli (such as optic flow, biological motion, etc.) compared to those used in the present experiments.

Although there is a fairly good correspondence between the incidence of direction-selective neurons and

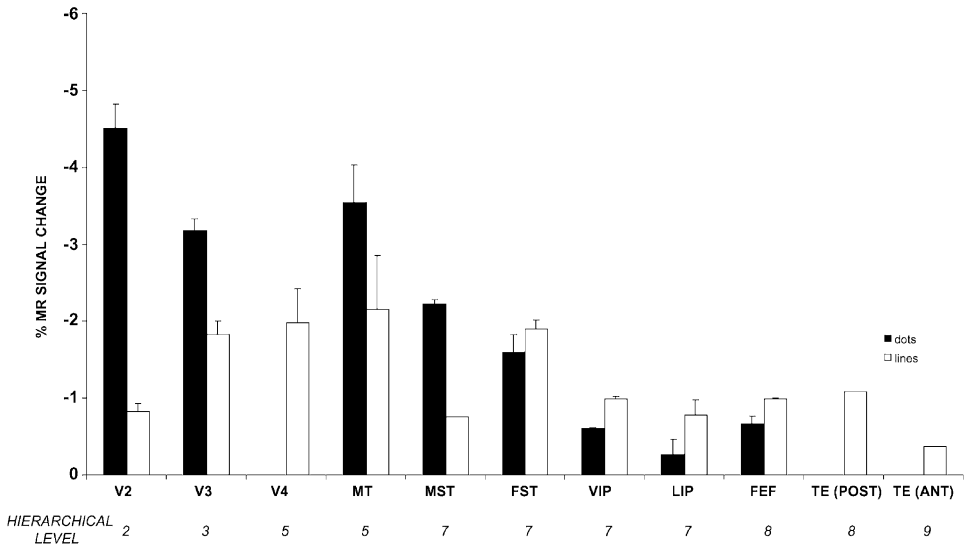

Figure 8. Overview of Motion Sensitivity in Function of Hierarchy and Stimulus Type

Percent MR signal changes for moving versus stationary dots (black bars) and lines (white bars). The visual areas are ordered along the *x* axis as a function of their hierarchical level (Felleman and Van Essen, 1991). Percent MR signal changes were calculated as (moving − stationary)/gray for seven (resampled) voxels around the local maximum ($p < 0.05$). Data are derived from the two hemispheres of monkey M1 and M3. Standard errors (calculated from data obtained in the four hemispheres) are indicated. TE (post) = posterior TE; TE (ant) = anterior TE.

the fMRI-based motion sensitivity, direction selectivity does not *entirely* explain the amplitude of the MR signal changes (see Figure 8). For example, direction selectivity in areas MST, FST, and VIP (>70% of their neurons are direction selective) surpasses that of area V3 (>40% of its neurons are direction selective), yet the latter area showed larger MR signal changes when comparing moving with stationary dots. This suggests that fMRI motion sensitivity is modulated by factors other than direction selectivity. One such factor is the hierarchical level of each cortical area. This probably reflects the increasing weight of extraretinal influences such as attention (e.g., Treue and Maunsell, 1996) and task-related factors (e.g., Shadlen and Newsome, 1996) in higher-order regions. Furthermore, as indicated by the difference in signal amplitude between moving dots and lines in most visual areas (see Figure 8), the modulation of the MR signal depends upon the stimulus type (density, type of texture, size, contrast, speed, etc.). Finally, since fMRI signals reflect mainly presynaptic activity (Logothetis et al., 2001) and depend on many nonneuronal physiological components, such as vascular density and vessel orientation, the amplitude of MRI signal changes (across different regions) cannot be used as an exact index of neuronal activities.

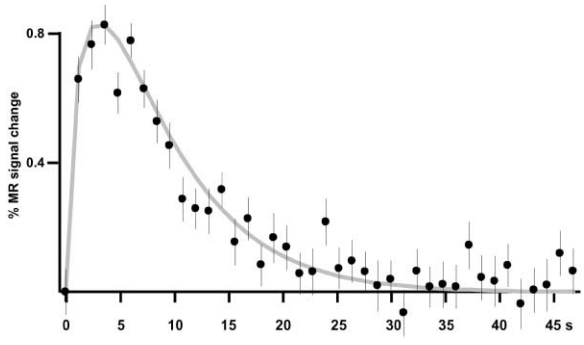

Figure 9. MION Impulse Response Function

MR signal change in visual cortex after the presentation of a flickering checkerboard stimulus (10 Hz, 28° diameter, 600 ms duration, TR = 74 ms/slice, 16 slices). A single γ function (gray) is fitted to the raw data. Vertical lines indicate SEM.

All the regions in which motion sensitivity was observed with moving dots have been assigned to the dorsal stream (Ungerleider and Mishkin, 1982; Maunsell and Newsome, 1987). We also observed motion sensitivity in a few regions which were not specifically implicated in motion processing previously (e.g., PIP, LIP, FEF, V4, and TE). These regions were motion sensitive for random lines only. Such random line stimuli have not yet been used in single-cell studies. However, Albright (1984) observed similar responses to random dots and single lines in area MT/V5.

In at least one of the two monkeys tested, we observed distinct bilateral motion-specific activations in the pulvinar and a region in the posterior bank of the lateral sulcus. An extrageniculate "motion" pathway has been postulated including the superior colliculus and the pulvinar (Rodman et al., 1990). This is supported by the profound connections between MT/V5 and the pulvinar (Ungerleider et al., 1984; Standage and Benevento, 1983). Moreover, a significant proportion of neurons in the pulvinar are direction selective (Petersen et al., 1985). Our knowledge is even more restricted with respect to visual processing in the lateral sulcus. As far as we know, only one group reported some degree of motion sensitivity in a multimodal region (PIVC) and a visual region (VPS) within this sulcus (Grüsser et al., 1990).

It could be argued that the observed motion sensitivity of FEF and also LIP might reflect overt and/or suppressed eye movements. Both the FEF and LIP are engaged before and during execution of saccades (Bizzi and Schiller, 1970; Andersen et al., 1990). In monkey M3, the effects of eye movements were explicitly removed by the statistical analysis (see Experimental Procedures). Since motion sensitivity in areas FEF and LIP was significant in both monkeys, it is unlikely that these activations reflect eye movements. Another factor might be the increased efforts to suppress eye movements when viewing moving stimuli. While it is unlikely that this factor contributes to the motion sensitivity observed in LIP (Gottlieb and Goldberg, 1999; Petit et al., 1995), it may well have contributed to the FEF activation. Single-cell studies (Bizzi, 1968; Hanes et al., 1998), electrical stimulation experiments (Burman and Bruce, 1997), and human imaging (Petit et al., 1995) implicate the FEF in the control of fixation. On the other hand, the FEF receives direct projections from motion-sensitive regions such as MT and MST (Schall et al., 1995), and FEF neurons signal target motion (Fukushima et al., 1999). Thus, stimulus motion as well as suppression of saccades may have contributed to the FEF activation in the present study.

Motion Sensitivity in the Primate Visual System: Comparing Human and Monkey fMRI

One goal of the present study was to compare brain activation in macaques with that in previous human studies, using fMRI as a common measurement technique. We found that many cortical areas (e.g., MT/V5+, V2, V3, regions in the IPS, and FEF) appeared functionally equivalent in macaques and humans (e.g., Zeki et al., 1991; Tootell et al., 1995; Sunaert et al., 1999; Goebel et al., 1998). This similarity may depend in part on the stimuli used, although the random dots used here were exactly the same as used by Sunaert et al. (1999). In as much as the motion sensitivity measured with fMRI in the macaque can be largely attributed to the activity of direction-selective neurons (see above), it is tempting to accept that this holds for humans as well.

When comparing two species that evolved independently over ~30 million years, one should also expect some species-specific differences in cortical organization. One such evolutionary difference suggested earlier was confirmed here. In human fMRI, retinotopically defined V3A is motion sensitive (Tootell et al., 1997; Goebel et al., 1998). On the other hand, macaque V3A showed no motion sensitivity at all in our fMRI measurements, in agreement with the single-cell results (Gaska et al., 1988; Joris et al., 1997). Such discrepancies between human and monkey visual cortical areas raise questions (which go beyond the scope of the present paper) about the extent to which functional and anatomical properties of a particular area may or may not deviate while retaining the same name. For example, in the case of area V3A, there are functional similarities (e.g., retinotopic organization) and anatomical similarities (V3A is located immediately anterior to area V3) but also functional dissimilarities (e.g., motion sensitivity) between the two species.

However, the question of homologies between humans and macaques *can be* explicitly addressed using monkey fMRI, which at least bridges the technical gap between human functional imaging and monkey single-cell studies. Furthermore, fMRI mapping will prove useful to guide physiological and anatomical studies in the monkey.

Experimental Procedures

Two male (M1 and M3) rhesus monkeys (3–4 kg) were used in both MION and BOLD experiments; a third monkey (M2) was used only in BOLD experiments. Prior to MR scanning, each monkey was implanted with an MR-compatible plastic headset attached to the skull by plastic T-like devices, plastic, and ceramic screws. The headset was covered by dental cement. All operations were performed under isoflurane (1.5%)/N_2O (50%)/O_2 (50%) or ketamine anesthesia (10 mg/kg, Ketalar®, i.m., Parke-Davis, Zaventem, Belgium) supplemented with xylazine (0.5 mg/kg, Rompun®, Bayer, Leverkusen, Germany). Antibiotics (50 mg/kg i.m., Kefzol®, Lilly, Brussels) and analgesics (4 mg/kg, i.m., Dolzam®, Zambon, Brussels) were given daily for 3–7 days following each surgery. The surgical procedures conformed to national, European, and National Institutes of Health (NIH) guidelines for the care and use of laboratory animals.

After recovery, the monkeys were adapted to physical restraint in a small plastic box (see Figure 1A), then habituated to the sounds of MR scanning in a "mock" MR bore. The monkeys were seated comfortably on their haunches, in the so-called "sphinx" position. The monkeys were water deprived during the period of testing, and behavioral control was achieved using operant conditioning techniques.

The three monkeys were trained to optimal performance on a high-acuity orientation discrimination task. The monkey had to interrupt a light path with its hand to indicate when a bar target changed its orientation from horizontal to vertical. Each correct response was rewarded with apple juice, delivered through a magnet-compatible juice delivery system (see Figure 1A). To ensure that the monkeys viewed the bar foveally, the bar was gradually reduced in size during training to 5 × 18 min arc. The bar was presented in the vertical orientation for only very brief periods (500 ms, intertrial interval (ITI) randomized between 500 and 2000 ms). Responses during the ITI were penalized by increasing the ITI by 1500 ms.

M3 was also trained on a fixation-only task. In this monkey, the high-acuity orientation discrimination task was used to accurately calibrate a pupil/corneal reflection tracking system (RK-726PCI, Iscan, Inc., Cambridge, MA). Once this eye tracking system was calibrated, we presented a fixation spot only instead of a fixation bar. The monkey was rewarded for maintaining fixation within a square-shaped central fixation window (2° on a side). The interval between rewards was systematically decreased (from 2500 to 500 ms) as the monkey maintained his fixation within the window.

After fixation performance reached asymptote (after 20 to 50 training sessions), each monkey (in its plastic restraint box) was placed into a horizontal bore, 1.5T Siemens Vision scanner, equipped with echoplanar imaging. A radial surface coil (10 cm diameter) was positioned immediately over the head (Figure 1A). This coil covered sufficiently the whole monkey brain, albeit with an ~30% signal intensity decrease along the dorsoventral axis of the brain. Before the scanning, MION (4–7 mg/kg) diluted in an isotonic saline buffer or sodium citrate (pH 8.0) was injected intravenously into the femoral vein.

The blood half-life of citrate-buffered MION, derived from the temporal decay of signal changes between visual and no visual stimulation after removal of the baseline drift, was 15.3 ± 3.5 hr. The optimal MION dose corresponds to the dose at which MR signal intensity is attenuated by a factor of ~2, relative to a preinjection baseline intensity (Mandeville et al., 1998). Since MION was injected prior to scanning, this dose (7 mg/kg on the first day and 4 mg/kg on subsequent days) was derived by comparing the average MR signal intensity after each MION injection to the average intensity of the preceding BOLD experiments.

Visual stimuli were projected from a Barco 6300 LCD projector

(640 × 480 pixels or 800 × 600 pixels, 60 Hz refresh rate) using customized optics (Buhl Optical) onto a screen which was positioned 15 cm (M1) or 54 cm (M3) in front of the monkey's eyes. Two types of stimuli were used: random texture patterns (referred to as dots) and random line patterns. These stimuli were either static or moved in one of eight randomly selected directions of planar motion. The dot stimuli were comprised of 50% black and 50% white dots (4.5 min arcmin/side) within a circular aperture of 14° diameter. During the motion condition, the direction changed randomly every 427 ms, and the uniform speed was adjusted to 2–6 deg/s. Random line stimuli consisted of nine interconnected lines of random length and orientation, also moving at a speed of 2–6 deg/s. In each experiment, the stimulus duration, eccentricity, and luminance were carefully equated across moving and stationary conditions. In all cases, the mean luminance was ~50 cd/m^2.

A block design was used in each scan session. Block duration was 24 s in the BOLD experiments and either 33 or 66 s in the MION experiments. The presentation order of the stimuli was randomized between scans, except for those experiments where we obtained average changes in MR signal as a function of time (referred to as time courses). Only scan sessions where the behavioral performance of the monkeys was excellent (>98% correct in the high-acuity orientation discrimination task for monkeys M1 and M2 or >85% fixation of the total scan duration for monkey M3) were considered for statistical analysis.

Each functional scan (time series) consisted of gradient-echo echoplanar whole-brain images (EPI; TR 3.321 s; TE = 32 ms; 64 × 64 matrix; 3 × 3 × 3 mm voxels; 32 coronal slices) using a Siemens Vision MR 1.5T scanner. The functional volumes were resliced to 1 mm^3 voxels and smoothed with a 2.5 mm^3 gaussian kernel, resulting in an overall smoothness of 4.3 × 4.8 × 4.4 mm full width at half-maximum. In additional experiments, we acquired higher resolution (using a Siemens Sonata MR 1.5T scanner) gradient-echo echoplanar whole-brain images (EPI; TR 2.3 s; TE = 32 ms; 64 × 64 matrix; 2 × 2 × 2 mm voxels; 16 or 32 coronal slices, smoothed with a 1.5 mm^3 gaussian kernel, yielding an overall smoothness at full width at half-maximum of 2.6 × 2.6 × 2.4 mm) during six (four MION and two BOLD) scan sessions. In addition to these functional scans, T1-weighted EPI's (0.84 × 0.84 × 3 mm voxels) were acquired in each daily session to match the functional data to the anatomy. The same scanning parameters were used in the BOLD and MION sessions. In a separate session, a 3D-MPRAGE volume (256 × 256 matrix; 112 slices; 1 × 1 × 1.25 mm voxel size) was acquired using a quadrature knee coil for each monkey while the monkey was anesthetized.

Data were analyzed using SPM99 and Freesurfer (flattening). After correcting for head motion, the functional volumes were rigidly registered with the anatomical volumes of the same monkey, in the Horsley-Clark stereotaxic space, globally scaled (Holmes et al., 1997), and high-pass filtered (cutoff = twice the shortest interval between repeated conditions). We verified that global scaling of the functional volumes (i.e., normalizing each functional volume to its mean value) increased the t values by 16% ± 4% in six visual regions for moving versus stationary stimulus comparisons. Realignment parameters of M1 and M3 as well as eye movement traces (subsampled to the TR and convolved with the HRF) of M3 were included as covariates of no interest in the general linear model used for statistical analysis (Friston et al., 1995). This way, we were able to dissociate eye movement-linked MR responses from stimulus-linked MR signal changes.

For the BOLD experiments, each stimulus epoch was represented as a box car model convolved by a hemodynamic response function equivalent to the default HRF (SPM99) value used for humans. Guided by the observation in the anesthetized rodent (Mandeville et al., 1999) that the kinetics of the MION-weighted signal has a rapid initial and a second slower phase following onset and offset of stimulation, we adjusted the parameters of the BOLD response function for the present MION experiments, modeled as a sum of two γ functions. This function was convolved with the box car model and adapted until a good fit ($\chi^2 = 7 \times 10^{-8}$) was obtained with the raw data.

In an additional control experiment in M3, we directly measured the MION impulse response function. To this end, a flickering checkerboard stimulus (10 Hz) was presented for 600 ms (TR 74 ms/slice, 16 slices, 2 × 2 × 2 mm voxels, Siemens, Sonata MR scanner) while the monkey fixated. The stimulus-evoked MR response (mean ± SEM) of 109 voxels (which were sampled in visual cortex) is shown in Figure 9. The gray curve represents a single γ function fitted ($\chi^2 = 7 \times 10^{-17}$) to the raw data. This function, which was slightly faster than expected from data obtained in anesthetized rodents, was convolved with the box car model for long epochs. This a posteriori-derived single γ function produced highly similar t maps as the double γ function which was actually used in the statistical analysis of the present experiment.

For each stimulus comparison, significant MR signal changes were assessed using a map of t scores (statistical parametric map). Unless stated otherwise, the threshold was set at $p < 0.05$, corrected for multiple comparisons. To identify motion-responsive regions, we used the local maxima in the statistical maps generated by the comparison (moving random dots versus stationary random dots) or (moving random lines versus stationary random lines). Because the "form" aspect of the stimulus was present in the two conditions of the subtraction, this feature on its own cannot account for the observed motion sensitivity. These local maxima were attributed to visual cortical areas using sulcal and gyral landmarks relative to previously published maps (e.g., Felleman and Van Essen, 1991).

Acknowledgments

This work was supported by grants of the Queen Elisabeth Foundation (GSKE), the National Research Council of Belgium (NFWO G3106.94 and NFWO G0112.00), the Flemish Regional Ministry of Education (GOA 95/6 and GOA 2000/11), the IUAP 4/22, EU contract QL63-CT-2000-30161 (Mapawamo), the MIND institute, and NIH RR14543A01 grants. The authors thank M. De Paep, W. Depuydt, A. Coeman, C. Fransen, P. Kayenberg, G. Meulemans, Y. Celis, and G. Vanparrijs for technical support. Furthermore, we thank E. Beatse and S. Sunaert for their support during the preliminary BOLD experiments. Special thanks are due to B. Fischl, and D. Tsao for their valuable discussions concerning the use of Freesurfer and the 3D reconstruction of M1. W.V. is a postdoctoral fellow of FWO-Flanders.

Received May 14, 2001; revised September 7, 2001.

References

Albright, T.D. (1984). Direction and orientation selectivity of neurons in visual area MT of the macaque. J. Neurophysiol. *52*, 1106–1130.

Andersen, R.A. (1997). Neural mechanisms of visual motion perception in primates. Neuron *18*, 865–872.

Andersen, R.A., Bracewell, R.M., Barash, S., Gnadt, J.W., and Fogassi, L. (1990). Eye position effects on visual, memory, and saccade-related activity in areas LIP and 7a of macaque. J. Neurosci. *10*, 1176–1196.

Bizzi, E. (1968). Discharge of frontal eye field neurons during saccadic and following eye movements in unanesthetized monkeys. Exp. Brain Res. *6*, 69–80.

Bizzi, E., and Schiller, P.H. (1970). Single unit activity in the frontal eye fields of unanesthetized monkeys during eye and head movement. Exp. Brain Res. *10*, 150–158.

Burman, D.D., and Bruce, C.J. (1997). Suppression of task-related saccades by electrical stimulation in the primate's frontal eye field. J. Neurophysiol. *77*, 2252–2267.

Colby, C.L., Duhamel, J.R., and Goldberg, M.E. (1993). Ventral intraparietal area of the macaque: anatomic location and visual response properties. J. Neurophysiol. *69*, 902–914.

Desimone, R., and Ungerleider, L.G. (1986). Multiple visual areas in the caudal superior temporal sulcus of the macaque. J. Comp. Neurol. *248*, 164–189.

Disbrow, E.A., Slutsky, D.A., Roberts-Timothy, P.L., and Krubitzer, L.A. (2000). Functional MRI at 1.5 tesla: A comparison of the blood oxygenation level-dependent signal and electrophysiology. Proc. Natl. Acad. Sci. USA *97*, 9718–9723.

Dubowitz, D.J., Chen, D.Y., Atkinson, D.J., Grieve, K.L., Gillikin, B.,

Bradley, W.G., Jr., and Andersen, R.A. (1998). Functional magnetic resonance imaging in macaque cortex. Neuroreport. *9*, 2213–2218.

Dupont, P., Orban, G.A., De Bruyn, B., Verbruggen, A., and Mortelmans, L. (1994). Many areas in the human brain respond to visual motion. J. Neurophysiol. *72*, 1420–1424.

Felleman, D.J., and Van Essen, D.C. (1987). Receptive field properties of neurons in area V3 of macaque monkey extrastriate cortex. J. Neurophysiol. *57*, 889–920.

Felleman, D.J., and Van Essen, D.C. (1991). Distributed hierarchical processing in the primate cerebral cortex. Cerebr. Cortex *1*, 1–47.

Friston, K.J., Holmes, A.P., Worsley, K.J., Poline, J.B., and Frackowiak, R.S.J. (1995). Statistical parametric maps in functional imaging: a general approach. Hum. Brain Mapp. *2*, 189–210.

Fukushima, K., Fukushima, J., and Sato, T. (1999). Vestibular-pursuit interactions: gaze-velocity and target-velocity signals in the monkey frontal eye fields. Ann. N.Y. Acad. Sci. *87*, 1248–1259.

Galletti, C., Fattori, P., Battaglini, P.P., Shipp, S., and Zeki, S. (1996). Functional demarcation of a border between areas V6 and V6A in the superior parietal gyrus of the macaque monkey. Eur. J. Neurosci. *8*, 30–52.

Gaska, J.P., Jacobson, L.D., and Pollen, D.A. (1988). Spatial and temporal frequency selectivity of neurons in visual cortical area V3A of the macaque monkey. Vision Res. *28*, 1179–1191.

Gegenfurtner, K.R., Kiper, D.C., and Levitt, J.B. (1997). Functional properties of neurons in macaque area V3. J. Neurophysiol. 77, 1906–1923.

Goebel, R., Khorram, S.D., Muckli, L., Hacker, H., and Singer, W. (1998). The constructive nature of vision: direct evidence from functional magnetic resonance imaging studies of apparent motion and motion imagery. Eur. J. Neurosci. *10*, 1563–1573.

Gottlieb, J., and Goldberg, M.E. (1999). Activity of neurons in the lateral intraparietal area of the monkey during an antisaccade task. Nat. Neurosci. *2*, 906–912.

Grüsser, O.-J., Pause, M., and Schreiter, U. (1990). Vestibular neurones in the parieto-insular cortex of monkeys *(Macaca fascicularis)*: visual and neck receptor responses. J. Physiol. *430*, 559–583.

Hanes, D.P., Patterson, W.F., and Schall, J.D. (1998). Role of frontal eye fields in countermanding saccades: visual, movement, and fixation activity. J. Neurophysiol. *79*, 817–834.

Hayashi, T., Konishi, S., Hasegawa, I., and Miyashita, Y. (1999). Mapping of somatosensory cortices with functional magnetic resonance imaging in anaesthetized macaque monkeys. Eur. J. Neurosci. *11*, 4451–4456.

Holmes, A.P., Josephs, O., Buchel, C., and Friston, K.J. (1997). Statistical modelling of low-frequency confounds in fMRI. Neuroimage *S480*

Joris, P.X., Raiguel, S.E., Xiao, D.K., and Orban, G.A. (1997). Responses in macaque area V3A to moving random dot patterns. Soc. Neurosci. Abstr. 23, 457.

Josephson, L., Groman, E.V., Menz, E., Lewis, J.M., and Bengele, H. (1990). A functionalized superparamagnetic iron oxide colloid as a receptor directed MR contrast agent. Magn. Reson. Imaging *8*, 637–646.

Lagae, L., Maes, H., Raiguel, S., Xiao, D.K., and Orban, G.A. (1994). Responses of macaque STS neurons to optic flow components: a comparison of areas MT and MST. J. Neurophysiol. *71*, 1597–1626.

Levitt, J.B., Kiper, D.C., and Movshon, J.A. (1994). Receptive fields and functional architecture of macaque V2. J. Neurophysiol. *71*, 2517–2542.

Logothetis, N.K., Guggenberger, H., Peled, S., and Pauls, J. (1999). Functional imaging of the monkey brain. Nat. Neurosci. *2*, 555–562.

Logothetis, N.K., Pauls, J., Augath, M., Trinath, T., and Oeltermann, A. (2001). Neurophysiological investigation of the basis of the fMRI signal. Nature *412*, 150–157.

Mandeville, J.B., and Marota, J.J. (1999). Vascular filters of functional MRI: spatial localization using BOLD and CBV contrast. Magn. Reson. Med. *42*, 591–598.

Mandeville, J.B., Marota, J.J., Kosofsky, B.E., Keltner, J.R., Weissleder, R., Rosen, B.R., and Weisskoff, R.M. (1998). Dynamic functional imaging of relative cerebral blood volume during rat forepaw stimulation. Magn. Reson. Med. *39*, 615–624.

Mandeville, J.B., Marota, J.J., Ayata, C., Zaharchuk, G., Moskowitz, M.A., Rosen, B.R., and Weisskoff, R.M. (1999). Evidence of a cerebrovascular postarteriole windkessel with delayed compliance. J. Cereb. Blood Flow Metab. *19*, 679–689.

Maunsell, J.H., and Newsome, W.T. (1987). Visual processing in monkey extrastriate cortex. Annu. Rev. Neurosci. *10*, 363–401.

Maunsell, J.H.R., and Van Essen, D.C. (1983). The connections of the middle temporal visual area (MT) and their relationship to a cortical hierarchy in the macaque monkey. J. Neurosci. *3*, 2563–2586.

Mikami, A., Newsome, W.T., and Wurtz, R.H. (1986). Motion selectivity in macaque visual cortex. I. Mechanisms of direction and speed selectivity in extrastriate area MT. J. Neurophysiol. *55*, 1308–1327.

Oram, M.W., and Perrett, D.I. (1994). Responses of anterior superior temporal polysensory (STPa) neurons to "biological motion" stimuli. J. Cogn. Neurosci. *6*, 99–116.

Orban, G.A. (1996). Physiology of motion and vision in primates. In Functional Neuroanatomy of motion and vision, G. Scotti and D. Le Bihan, eds. (Milan: Edizioni del Centauro-Udine), pp. 23–28.

Orban, G.A., Kennedy, H., and Bullier, J. (1986). Velocity sensitivity and direction selectivity of neurons in areas V1 and V2 of the monkey: influence of eccentricity. J. Neurophysiol. *56*, 462–480.

Peterhans, E., and Watson, J.D.G. (1993). Functional organization of area V2 in the alert macaque. Eur. J. Neurosci. *5*, 509–524.

Petersen, S.E., Robinson, D.L., and Keys, W. (1985). Pulvinar nuclei of the behaving rhesus monkey: visual responses and their modulation. J. Neurophysiol. *54*, 867–886.

Petit, L., Tzourio, N., Orssaud, C., Pietrzyk, U., Berthoz, A., and Mazoyer, B. (1995). Functional neuroanatomy of the human visual fixation system. Eur. J. Neurosci. *7*, 169–174.

Rodman, H.R., Gross, C.G., and Albright, T.D. (1990). Afferent basis of visual response properties in area MT of the macaque. II. Effects of superior colliculus removal. J. Neurosci. *10*, 1154–1164.

Schaffer, B.K., Linker, C., Papisov, M., Tsai, E., Nossiff, N., Shibata, T., Bogdanov, A., Brady, T.J., and Weissleder, R. (1993). MION-ASF: biokinetics of an MR receptor agent. Magn. Reson. Imaging *11*, 411–417.

Schall, J.D., Morel, A., King, D.J., and Bullier, J. (1995). Topography of visual cortex connections with frontal eye field in macaque: convergence and segregation of processing streams. J. Neurosci. *15*, 4464–4487.

Shadlen, M.N., and Newsome, W.T. (1996). Motion perception: Seeing and deciding. Proc. Natl. Acad. Sci. USA *93*, 628–633.

Siegel, R.M., and Read, H.L. (1997). Analysis of optic flow in the monkey parietal area 7a. Cerebr. Cortex *7*, 327–346.

Standage, G.P., and Benevento, L.A. (1983). The organization of connections between the pulvinar and visual area MT in the macaque monkey. Brain Res. *262*, 288–294.

Stefanacci, L., Reber, P., Costanza, J., Wong, E., Buxton, R., Zola, S., Squire, L., and Albright, T. (1998). fMRI of monkey visual cortex. Neuron *20*, 1051–1057.

Sunaert, S., Van Hecke, P., Marchal, G., and Orban, G.A. (1999). Motion-responsive regions of the human brain. Exp. Brain Res. *127*, 355–370.

Tanaka, K., Hikosaka, K., Saito, H., Yukie, M., Fukada, Y., and Iwai, E. (1986). Analysis of local and wide-field movements in the superior temporal visual areas of the macaque monkey. J. Neurosci. *6*, 134–144.

Tanaka, K., Sugita, Y., Moriya, M., and Saito, H. (1993). Analysis of object motion in the ventral part of the medial superior temporal area of the macaque visual cortex. J. Neurophysiol. *69*, 128–142.

Tootell, R.B., Reppas, J.B., Kwong, K.K., Malach, R., Born, R.T., Brady, T.J., Rosen, B.R., and Belliveau, J.W. (1995). Functional analysis of human MT and related visual cortical areas using magnetic resonance imaging. J. Neurosci. *15*, 3215–3230.

Tootell, R.B., Mendola, J.D., Hadjikhani, N.K., Ledden, P.J., Liu, A.K., Reppas, J.B., Sereno, M.I., and Dale, A.M. (1997). Functional analysis of V3A and related areas in human visual cortex. J. Neurosci. *17*, 7060–7078.

Treue, S., and Maunsell, J.H. (1996). Attentional modulation of visual motion processing in cortical areas MT and MST. Nature *382*, 539–541.

Ungerleider, L.G., and Mishkin, M. (1982). Analysis of Visual Behavior (Cambridge, MA: The MIT Press).

Ungerleider, L.G., Desimone, R., Galkin, T.W., and Mishkin, M. (1984). Subcortical projections of area MT in the macaque. J. Comp. Neurol. *223*, 368–386.

Van Bruggen, N., Busch, E., Palmer, J.T., Williams, S.P., and de Crespigny, A. (1998). High-resolution functional magnetic resonance imaging of the rat brain: mapping changes in cerebral blood volume using iron oxide contrast media. J. Cereb. Blood Flow Metab. *18*, 1178–1183.

Vanduffel, W., Beatse, E., Sunaert, S., Van Hecke, P., Tootell, R.B.H., and Orban, G.A. (1998). Functional magnetic resonance imaging in an awake rhesus monkey. Soc. Neurosci. Abstr. *24*, 11.

Weissleder, R., Elizondo, G., Wittenberg, J., Rabito, C.A., Bengele, H.H., and Josephson, L. (1990). Ultrasmall superparamagnetic iron oxide: characterization of a new class of contrast agents for MR imaging. Radiology *175*, 489–493.

Zeki, S., Watson, J.D.G., Lueck, C.J., Friston, K.J., Kennard, C., and Frackowiak, R.S.J. (1991). A direct demonstration of functional specialization in human visual cortex. J. Neurosci. *11*, 641–649.